Editors' Suggestion

## Twisted coupled wire model for a moiré sliding Luttinger liquid

Yichen Hu, 1 Yuanfeng Xu, 1,2 and Biao Lian 1 <sup>1</sup>Department of Physics, Princeton University, Princeton, New Jersey 08544, USA <sup>2</sup>Center for Correlated Matter and School of Physics, Zhejiang University, Hangzhou 310058, China



(Received 18 October 2023; revised 24 October 2024; accepted 28 October 2024; published 14 November 2024)

Recent experiments in twisted bilayer WTe<sub>2</sub> revealed the existence of anisotropic Luttinger liquid behavior. To generically characterize such anisotropic twisted bilayer systems, we study a model of a twisted bilayer of two-dimensional (2D) arrays of coupled wires, which effectively form an array of coupled moiré wires. We solve the model by the transfer matrix method, and identify quasi-1D electron bands in the system at small twist angles. With electron interactions added, we show that the moiré wires have an effective Luttinger parameter  $g_{\text{eff}}$  lower than that of the microscopic wires. This leads to a sliding Luttinger liquid (SLL) temperature regime, in which power-law current voltage relations arise. For parameters partly estimated from WTe2, a microscopic interaction  $U \sim 3$  eV yields a temperature regime of SLL similar to that in the WTe<sub>2</sub> experiments.

DOI: 10.1103/PhysRevB.110.L201106

One-dimensional (1D) interacting electrons form Luttinger liquids [1–6], which show non-Fermi-liquid physics such as spin-charge separation and power-law voltage-current relations violating the Ohm's law. In highly anisotropic 2D electron systems, it was proposed that interactions can lead to a sliding Luttinger liquid (SLL) phase or regime [7–25], which shows quasi-1D physics analogous to the 1D Luttinger liquid [26–29]. Recent studies of moiré systems of twisted homobilayer or heterobilayer 2D materials have enabled engineering of a rich variety of 2D electron systems, such as flat bands with strong interactions [5,29-46]. Intriguingly, in the twisted bilayer WTe2, which hosts a rectangular moire pattern, transport experiments [28,29] reveal a phase that exhibits (1) a strong in-plane electronic anisotropy, (2) a power-law scaled conductance in the hard direction, and (3) a nonlinear differential resistance that vanishes at zero bias in the easy direction. The phenomena strongly suggests quasi-1D physics in a SLL regime. The tunability of moiré systems may allow a thorough exploration of the physics of SLLs. Therefore, it is important to understand theoretically the mechanism of quasi-1D SLLs from twisted bilayer anisotropic systems, and to investigate its dependence on twist angles and interaction strengths.

In this paper, we study a model of a twisted bilayer of 2D arrays of coupled wires, which effectively forms a network model with interwire and interlayer hoppings. The goal of the model is to give a simplified generic description of twisted bilayer anisotropic systems, and investigate the emergence of an array of coupled moiré wires showing SLL physics. At small twist angles, the model can be solved from the real space transfer matrix, which directly gives the Fermi surface of moiré bands at the Fermi energy. We find that, compared to the microscopic coupled wires, the emergent coupled moiré wires show much smaller Luttinger parameter geff, implying much stronger correlation effects. For parameters partly estimated from WTe2, a microscopic interaction  $U \gtrsim 3$  eV yields an SLL temperature regime around that in experiments.

The single-particle model. Monolayer WTe<sub>2</sub> has an anisotropic crystal structure and an anisotropic band structure, as shown in Fig. 1(a). In the valence band, which is relevant to SLL experimentally [28,29], the W atom orbitals dominate. In real space, the W atoms approximately form arrays of quasi-1D wires [along the horizontal direction in Fig. 1(b)]. In twisted bilayer WTe<sub>2</sub>, the W atom quasi-1D wires of the two layers form a moiré pattern in Fig. 1(b), which visually shows effective vertical moiré wires at a larger length scale.

To give a generic simplified single-particle model of an anisotropic moiré system such as twisted bilayer WTe<sub>2</sub>, we approximate each layer by an array of coupled wires with interwire distance l as shown in Fig. 1(c), where the blue and red wires are in the upper and lower layers, respectively. The two layers differ by a twist angle  $\theta$ . We assume the electrons (or holes via a particle-hole transformation) in each wire have a quadratic dispersion with an effective mass m, and a hopping  $-t_{\perp}$  between two nearest neighbor wires in each layer. Since the relevant hole band in WTe<sub>2</sub> is around the  $\Gamma$  point, the spin-orbital coupling can be neglected (as is known for transition-metal dichalcogenides [47,48]), and thus we can choose  $t_{\perp}$  to be real. As shown in Fig. 1(c), the wires of the two layers cross at positions with x coordinates  $x = n_x a_x$ , where  $n_x \in \mathbb{Z}$  and  $a_x = \frac{l}{2\sin(\theta/2)}$ . The vertical distance between two neighboring wires in each layer is  $a_y = \frac{l}{\cos(\theta/2)}$ . At each crossing of two wires from two layers [Fig. 1(d)], we assume a delta function intralayer potential of strength  $\lambda$  and a delta function interlayer hopping of strength  $\lambda'$ . For small twist angle  $\theta$ , we can approximate the coordinate along each wire by x, and we use  $\psi_{\alpha,n_y}(x)$  to denote the wave function in the  $n_v$ th wire  $(n_v \in \mathbb{Z})$  in layer  $\alpha = \pm$ . Note that because of the relative twisting, the  $n_v$ th wire in layer  $\alpha$  crosses with the  $(n_y - \alpha n_x)$ th wire in layer  $-\alpha$  at  $x = n_x a_x$ . The

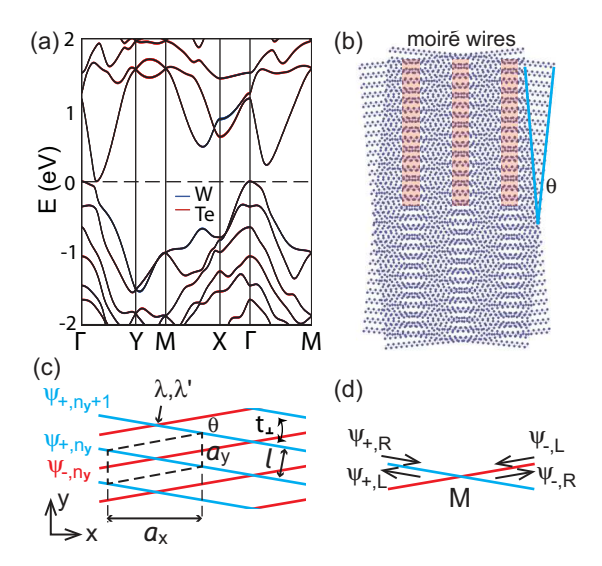


FIG. 1. (a) DFT band structure of monolayer WTe<sub>2</sub>, showing domination by W orbitals in the valence band around the  $\Gamma$  point. (b) W atom positions in twisted bilayer WTe<sub>2</sub>, and illustration of the emergent moiré wires. (c) Twisted network model consisting of two arrays of coupled wires with a twist angle  $\theta$ . Dotted lines encircle a moiré unit cell. (d) Zoom-in around a single interlayer intersection point, across which the wave functions are related by transfer matrix M.

single-particle Shrödinger equation at energy E (measured from band bottom) is then

$$E\psi_{\alpha,n_{y}} = \left(2t_{\perp} - \frac{\hbar^{2}\partial_{x}^{2}}{2m}\right)\psi_{\alpha,n_{y}} - t_{\perp}(\psi_{\alpha,n_{y}+1} + \psi_{\alpha,n_{y}-1}) + \delta(x - n_{x}a_{x})(\lambda\psi_{\alpha,n_{y}} + \lambda'\psi_{-\alpha,n_{y}-\alpha n_{x}}).$$
(1)

While this oversimplified model does not correspondi to a concrete material, our goal is to understand how moiré patterns generically give rise to SLL physics. Hereafter, to reflect the physics of twisted bilayer WTe2 as much as possible, we take l = 0.627 nm, interlayer distance  $a_z = 0.77$  nm, and  $m = 0.38m_e$  where  $m_e$  is the bare electron mass, as estimated for the W atom chains in WTe<sub>2</sub> from density functional theory (DFT). For the effective interwire hoppings, we take  $t_{\perp} = 20 \text{meV}$ ,  $\lambda = 10 \text{ meV}$  nm, and  $\lambda' = 20 \text{ meV}$  nm, based on the order of magnitude of direct hopping between W atoms in DFT [see Supplemental Material (SM) [49] Secs. IV and V for details (see also references [50–52] therein)]. However, we do not expect the above effective parameters to characterize WTe<sub>2</sub> quantitatively, which experimentally shows substantial deviations from DFT in some aspects, possibly due to strong interactions [53–60]

The Schrödinger Eq. (1) for small  $\theta$  can be most easily solved by the transfer matrix method. We consider the transfer matrix in the x direction for a state with energy E and quasi-momentum  $q_y$  in the y direction. For  $(n_x - 1)a_x < x < n_x a_x$ , such a state takes the form

$$\begin{split} \psi_{\alpha,n_{y}}(x) &= e^{iq_{y}a_{y}(n_{y} - \frac{\alpha}{2}n_{x})}\widetilde{\psi}_{\alpha,q_{y}}^{n_{x}}(x), \\ \widetilde{\psi}_{\alpha,q_{y}}^{n_{x}}(x) &= e^{ik(x - n_{x}a_{x})}\varphi_{\alpha,q_{y}}^{n_{x},R} + e^{-ik(x - n_{x}a_{x})}\varphi_{\alpha,q_{y}}^{n_{x},L}, \end{split} \tag{2}$$

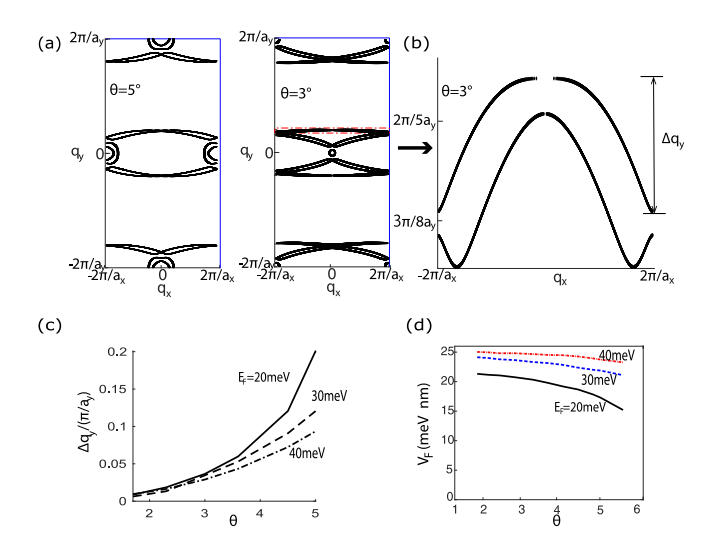


FIG. 2. (a) Fermi surface solved for  $\theta=5^\circ$  (left) and  $\theta=3^\circ$  (right) twisted model with Fermi energy  $E_F=30$  meV, using the transfer matrix method [with parameters given below Eq. (1)]. (b) Zoomed-in plot of the red dotted region of the  $3^\circ$  Fermi surface in (a).  $\Delta q_y$  characterizes the flatness of  $q_x$ -direction dispersion of the band. (c)  $\frac{\Delta q_y}{\pi/a_y}$  versus  $\theta$  for different  $E_F$ . (d) Fermi velocity  $v_F$  versus angle  $\theta$  for different Fermi energies  $E_F$ .

where  $k=\hbar^{-1}\sqrt{2m\{E+2t_{\perp}[\cos(q_ya_y)-1]\}}$  is the free momentum along the wire, and  $\varphi_{\alpha,q_y}^{n_x,R}$  and  $\varphi_{\alpha,q_y}^{n_x,L}$  are the right-moving and left-moving amplitudes, respectively. By reorganizing the wave function into a four-component vector  $\Psi_{q_y,n_x}=(\varphi_{+,q_y}^{n_x,L},\varphi_{+,q_y}^{n_x,R},\varphi_{-,q_y}^{n_x,R})^T$ , the Shrödinger equation can be reformulated into the transfer matrix equation (SM [49] Sec. I)

$$\Psi_{q_{y},n_{x}+1} = T(E, q_{y})\Psi_{q_{y},n_{x}}.$$
(3)

The transfer matrix can be further decomposed into two parts,  $T(E, q_y) = Q(E, q_y)M(E, q_y)$ , where  $Q(E, q_y) = \text{diag}(e^{-ika_x}, e^{ika_x}, e^{-ika_x}, e^{ika_x})$  is the diagonal propagation matrix, and one can show that

$$M(E, q_y) = \begin{pmatrix} \left(\sigma_0 - \frac{i\lambda'm}{k}s_0\right)e^{i\frac{q_y}{2}} & -\frac{i\lambda m}{k}s_0e^{i\frac{q_y}{2}} \\ -\frac{i\lambda m}{k}s_0e^{-i\frac{q_y}{2}} & \left(\sigma_0 - \frac{i\lambda'm}{k}s_0\right)e^{-i\frac{q_y}{2}} \end{pmatrix}$$
(4)

is the scattering matrix at the node, where  $\sigma_0$  is the 2 × 2 identity matrix, and  $s_0 = \sigma_z + i\sigma_y$  in terms of the 2 × 2 Pauli matrices  $\sigma_{x,y,z}$ .

One can solve the eigenvectors of the transfer matrix  $T(E, q_y)$ , and we denote the eigenvalue as  $e^{iq_x a_x}$ :

$$T(E, q_{y})\widetilde{\Psi}_{q_{y}, q_{x}} = e^{iq_{x}a_{x}}\widetilde{\Psi}_{q_{y}, q_{y}}.$$
 (5)

If  $q_x$  is real, the eigenvector  $\widetilde{\Psi}_{q_y,q_x}$  gives an eigenstate of the Shrödinger Eq. (1), with quasimomentum  $q_x$  in the x direction and  $q_y$  in the y direction.

Taking  $E = E_F$  to be the Fermi energy, the above procedure naturally gives the Fermi surface of the band structure in the quasimomentum  $(q_x, q_y)$  space. The transfer matrix is thus advantageous if one focuses on the low energy states near the Fermi surface. Figure 2(a) shows the Fermi surface (black lines) calculated for  $E_F = 30$  meV at 5° (left) and 3°

(right). Figure 2(b) shows zoomed in image of bands boxed in red dotted lines in 3° Fermi surface. As shown in Fig. 2(a), there are Fermi surfaces forming a periodic loop in the  $q_x$ direction, indicating that these bands are highly quasi-1D, with effective coupled moiré wires as shown in Fig. 1(b). We focus on the band with the flattest Fermi surface. We characterize the anisotropy of the band by the dimensionless number  $a_v \Delta q_v / \pi$ , where  $\Delta q_v$  is the width of  $q_v$  spanned by the Fermi surface dispersion shown in Fig. 2(b). This anisotropy as a function of twist angle  $\theta$  for different  $E_F$  is shown by the black lines in Fig. 2(c). We note that such quasi-1D Fermi surfaces forming loops in  $q_x$  only occur below a certain twist angle  $\theta_c$ , for instance,  $\theta_c \approx 6.3^{\circ}$  for  $E_F = 30$  meV. Moreover, we can numerically calculate the Fermi velocity of the band  $v_F = dE/dq_v$  at  $q_x = 0$  by slightly varying E and  $q_v$ . The Fermi velocity  $v_F$  as a function of  $\theta$  for different  $E_F$  is given

We can estimate the effective y direction hopping energy of a moiré wire in Fig. 1(b) by  $\widetilde{t}_{\parallel} = \pi v_F/a_y$ , using the fact that  $\pi/a_y$  is the half Brillouin zone size in the y direction. The effective hopping across two nearest moiré wires can be estimated by  $\widetilde{t}_{\perp} = v_F \Delta q_y$ , which is the energy scale inducing the Fermi surface dispersion of width  $\Delta q_y$ . Therefore, the anisotropy of effective coupled moiré wires in Fig. 2(c) is also equal to

$$\widetilde{t}_{\perp}/\widetilde{t}_{\parallel} = a_{\nu} \Delta q_{\nu}/\pi. \tag{6}$$

The smaller  $\tilde{t}_{\perp}/\tilde{t}_{\parallel}$  is, the more quasi-1D in y direction the moiré band is.

Interaction effect. We now add electron-electron interaction to the model, and examine the emerging SLL physics in the moiré scale. The emergent quasi-1D moiré bands in the above model provide fertile ground for interaction induced correlations. In the microscopic lattice scale, we consider a generic spin-independent anisotropic screened repulsive interaction between two electrons with distance **r** (both intralayer and interlayer):

$$V_I(\mathbf{r}) = U \exp\left(-\sqrt{\frac{x^2}{x_0^2} + \frac{y^2}{y_0^2} + \frac{z^2}{z_0^2}}\right). \tag{7}$$

In a 2D Thomas-Fermi screening model of Coulomb interaction, the screening length is estimated as  $r_0 = \frac{2\pi\epsilon_r\epsilon_0\hbar^2}{e^2m}$  along a direction with effective mass m, where e is the electric charge. Along the x direction, taking  $\epsilon_r \approx 10$  (which is approximately the value for WTe<sub>2</sub> [61]), and effective mass  $m=0.38m_e$ , one arrives at a screening length  $x_0 \sim 1$  nm. The quasi-1D nature (along the x direction) of the microscopic system gives heavier effective masses (by approximately one order of magnitude) along the y and z directions, so we take  $y_0=5$  nm,  $z_0=10$  nm. We note that for low carrier densities with which we are concerned, the bare interaction energy scale is likely larger than the electron kinetic energy, so the Thomas-Fermi model may overestimate the screening. Nevertheless, as a model study, we fix  $x_0$ ,  $y_0$ , and  $z_0$  as above, and leave the microscopic interaction U as a tuning parameter. For reference, taking  $V_I(x_0,0,0) \sim \frac{e^2}{4\pi\epsilon_0 x_0}$  yields a U of order 5 eV.

For a 1D moiré wire, the electrons with interaction become a Luttinger liquid with spin-charge separation. The charge

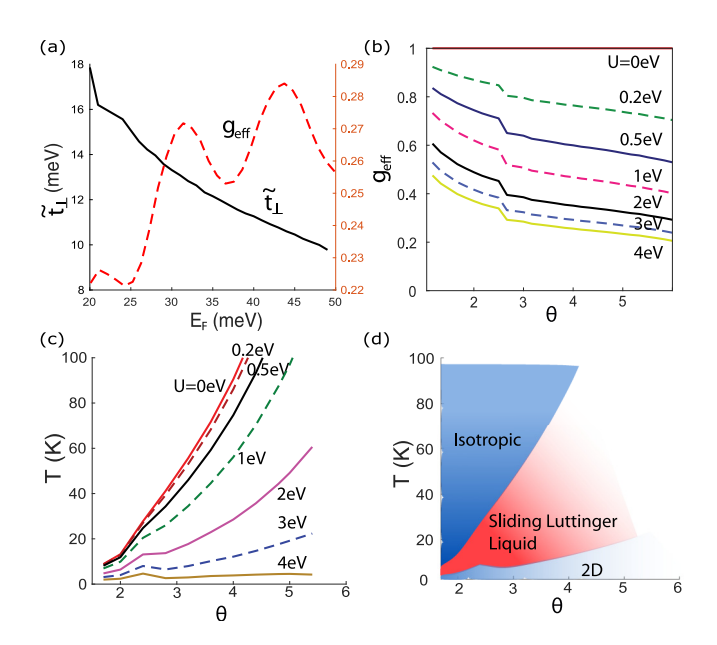


FIG. 3. (a) Plots of effective Luttinger parameter  $g_{\rm eff}$  and interwire coupling  $\tilde{t}_{\perp}$  vs Fermi energy  $E_F$  at 5° and U=3 eV. The left y axis shows  $\tilde{t}_{\perp}$  and the right y-axis shows  $g_{\rm eff}$ . (b) Plot of  $g_{\rm eff}$  versus twist angle  $\theta$  for different U at Fermi energy  $E_F=30$  meV. (c) The lower-bound SLL temperature  $T_*$  vs  $\theta$  for different U at Fermi energy  $E_F=30$  meV. (d) Phase diagram for a twisted system at different angles  $\theta$  for U=3 eV at Fermi energy  $E_F=30$  meV. The upper and lower boundaries are crossover temperatures  $T_0$  and  $T_*$ , respectively.

Luttinger parameter  $g_{\text{eff}}$  and spin Luttinger parameter  $g_{\text{eff},s}$  are given by [4,62]

$$g_{\text{eff}} = \sqrt{\frac{2\pi v_F + \widetilde{V}(2q_F)}{2\pi v_F + 2\widetilde{V}(0) - \widetilde{V}(2q_F)}},$$

$$g_{\text{eff},s} = \sqrt{\frac{2\pi v_F + \widetilde{V}(2q_F)}{2\pi v_F - \widetilde{V}(2q_F)}},$$
(8)

where  $\widetilde{V}(0)$  and  $\widetilde{V}(2q_F)$  are the interaction strength in the quasimomentum  $q_y$  space for scattering with zero momentum change (forward scattering) and  $2q_F$  momentum change (back scattering), respectively (see SM [49] Sec. II), and  $v_F = dE/dq_y$  is the Fermi velocity. For repulsive interaction, one usually has  $\widetilde{V}(0) > \widetilde{V}(2q_F)$  and  $\widetilde{V}(0) > 0$ , thus  $g_{\rm eff} < 1$ . For the parameters we choose, we find  $|\widetilde{V}(2q_F)| \sim 10^{-3}\widetilde{V}(0) \ll v_F$ , so the spin Luttinger parameter is always approximately  $g_{\rm eff,s} \approx 1$ .

We average over pairs of Fermi surface states at quasimomenta  $(q_x, \pm q_F(q_x))$  to obtain the average charge Luttinger parameter  $g_{\rm eff}$ . Figure 3(a) shows  $g_{\rm eff}$  as a function of  $E_F$  calculated for U=3 eV and twist angle  $\theta=5^\circ$ , which is below 0.3. The effective hopping  $\widetilde{t}_\perp$  between neighboring moiré wires is also plotted. Figure 3(b) shows how  $g_{\rm eff}$  depends on the interaction strength U as a function of  $\theta$ , where  $E_F=30$  meV. We find that  $g_{\rm eff}$  increases as  $\theta$  decreases. This is because the width  $a_x$  of a moiré wire increases as  $\theta$  decreases, and thus two electrons in the moiré wire have less chance to scatter with each other, leading to a weaker effective interaction. In comparison, for a microscopic decoupled wire

in a monolayer, which has a Fermi momentum  $k_F = \sqrt{2mE_F}$ , we can estimate its microscopic Luttinger parameter g similarly to Eq. (8), which is generically larger ( $g \gtrsim 0.6$ ) than the moiré effective Luttinger parameter  $g_{\rm eff}$  here given the same U.

The moiré SLL regime. The temperature regime for SLL physics depends on the effective moiré parameters  $\tilde{t}_{\perp}$ ,  $\tilde{t}_{\parallel}$ , and  $g_{\rm eff}$  [10,11,25,63], which we explain below. Without the interwire hopping  $\tilde{t}_{\perp}$ , and setting  $g_{\rm eff,s}=1$ , each moiré wire along the y direction has a zero-temperature 1D Luttinger liquid Green's function following [64]

$$G_{\zeta}^{1D}(y,t) = \langle \mathcal{T}\hat{\psi}_{n_{x},\zeta}(y,t)\hat{\psi}_{n_{x},\zeta}^{\dagger}(0,0)\rangle$$

$$= \frac{1}{2\pi}(y - \zeta v_{c}t + i\zeta 0^{+})^{-\frac{1}{2}}(y - \zeta v_{s}t + i\zeta 0^{+})^{-\frac{1}{2}}$$

$$\times \left[y^{2} - v_{c}^{2}(t - i0^{+})^{2}\right]^{-\frac{\eta}{2}}, \tag{9}$$

where  $\zeta=\pm$  stand for the modes moving in the  $\pm y$  directions, resepectively, the charge mode has velocity  $v_c=\frac{1}{2\pi}\sqrt{[2\pi v_F+\widetilde{V}(0)]^2-[\widetilde{V}(2q_F)-\widetilde{V}(0)]^2}$ , the spin mode has velocity  $v_s=\frac{1}{2\pi}\sqrt{4\pi^2v_F^2-\widetilde{V}(2q_F)^2}\approx v_F$ , and the anomalous exponent  $\eta=(g_{\rm eff}+g_{\rm eff}^{-1}-2)/4$ . In particular,  $\eta=0$  in the noninteracting  $g_{\rm eff}=1$  limit. At low energies, the local density of states (spectral weight) scales as

$$\rho(\omega) = -\frac{1}{\pi} \operatorname{Im} \sum_{\zeta = +} \widetilde{G}_{\zeta}^{1D}(0, \omega) \propto \omega^{\eta}, \tag{10}$$

where  $\widetilde{G}_{\zeta}^{1D}(y,\omega)$  is the Fourier transform of Eq. (9) in time t. As can be seen by a simple power counting, the full Fourier transform of Eq. (9) in both y and t scales as  $G_{\zeta}^{1D}(q,\omega) = \omega^{\eta-1}\widetilde{t}_{\parallel}^{-\eta}f(q/\omega)$  (which has the unit of inverse of energy), where f(x) is some dimensionless function of order unity.

With the effective interwire hopping  $\tilde{t}_{\perp}$ , the hopping among different moiré wires can be incorporated as a self-energy correction to Eq. (9). The zero-temperature Green's function is perturbatively given by a Schwinger-Dyson equation [63]:

$$G_{\zeta}(q,\omega) \approx G_{\zeta}^{1D}(q,\omega) + \widetilde{t}_{\perp} G_{\zeta}^{1D}(q,\omega) G_{\zeta}(q,\omega)$$

$$\approx \frac{G_{\zeta}^{1D}(q,\omega)}{1 - \widetilde{t}_{\perp} G_{z}^{1D}(q,\omega)}.$$
(11)

In the case  $0 \leqslant \eta < 1$ , for which the interaction is not too strong,  $G_{\zeta}^{\rm 1D}(q,\omega) \propto \omega^{\eta-1} \widetilde{t}_{\parallel}^{-\eta}$  diverges in the low energy limit  $\omega \to 0$ . Clearly, the perturbation estimation Eq. (11) will break down when  $\widetilde{t}_{\perp} G_{\zeta}^{\rm 1D}(q,\omega) \sim \widetilde{t}_{\perp} \widetilde{t}_{\parallel}^{-\eta} \omega^{\eta-1} > 1$ , namely, when the energy scale  $\omega < \widetilde{t}_{\perp} (\widetilde{t}_{\perp} / \widetilde{t}_{\parallel})^{\frac{\eta}{1-\eta}}$ . In this case,  $\widetilde{t}_{\perp}$  can no longer be treated as a perturbation, and the system will behave as an intrinsically 2D system. For energy scales  $\omega > \widetilde{t}_{\perp} (\widetilde{t}_{\perp} / \widetilde{t}_{\parallel})^{\frac{\eta}{1-\eta}}$ , the Green's function in Eq. (11) resembles that of the 1D Luttinger liquid closely, and SLL quasi-1D behaviors are expected. In the case  $\eta \geqslant 1$ ,  $G_{\zeta}^{\rm 1D}(q,\omega)$  does not diverge as  $\omega \to 0$ , and thus the SLL quasi-1D behavior persists down to  $\omega = 0$ .

At finite temperature, the temperature T plays the role of the energy scale of the system, and thus the 1D Luttinger liquid Green's function  $G_{\zeta}^{1D}(q,\omega) \propto (k_B T)^{\eta-1} \widetilde{t}_{\parallel}^{-\eta}$  in the low energy limit  $\omega \to 0$ , where  $k_B$  is the Boltzmann con-

stant. Therefore, the quasi-1D SLL physics can only exist for temperatures  $T > T_*$ , where the lower bound crossover temperature for  $0 \le \eta < 1$  is

$$T_* \approx k_B^{-1} \widetilde{t}_{\perp} (\widetilde{t}_{\perp} / \widetilde{t}_{\parallel})^{\frac{\eta}{1-\eta}}. \tag{12}$$

For  $\eta \geqslant 1$ , the SLL physics will persist down to  $T_* = 0$ .

In the SLL temperature regime  $T > T_*$ , the transverse conductivity  $\sigma_{\perp}$  across the moiré wires [namely, in the x direction in Fig. 1(c)] at temperature T is known to exhibit a power-law scaling [7–12,25], Treating  $\tilde{t}_{\perp}$  as perturbation,  $\sigma_{\perp}$  is governed by the Kubo formula for tunneling between two neighboring wires:

$$\sigma_{\perp}(\omega, T) \propto \widetilde{t}_{\perp}^{2} \int dy \int d\omega' \frac{n_{f}(\omega' + \omega) - n_{f}(\omega')}{\omega} \times \operatorname{Im} \widetilde{G}_{\alpha}^{1D}(y, \omega') \operatorname{Im} \widetilde{G}_{\alpha}^{1D}(y, \omega + \omega') \times \widetilde{t}_{\perp}^{2} T^{2\eta - 1} F\left(\frac{\omega}{T}\right), \tag{13}$$

where F(x) approaches 1 as  $x \to 0$ , and scales as  $x^{2\eta-1}$  as  $x \gg 1$ . For transverse transport measurement with voltage V between two neighboring moiré wires, the energy scale  $\omega$  can be identified with V. Therefore, the transverse conductivity

$$\sigma_{\perp}(V,T) \propto \begin{cases} V^{2\eta-1} & (eV > k_B T), \\ T^{2\eta-1} & (eV < k_B T), \end{cases}$$
(14)

which is the key feature of SLL. The longitudinal conductivity  $\sigma_{\parallel}$  along the moiré wires [the y direction in Fig. 1(c)] is expected to be similar to that of the 1D Luttinger liquid, which increases as T decreases in the disorderless limit (diverging at T=0, if temperature T could reach zero).

Physically, the SLL regime cannot persist to arbitrarily high temperature, since the Luttinger liquid theory is only valid at low energies. In the literature [4,65], it is assumed that the upper bound temperature is  $T_0 \sim \tilde{t}_{\parallel}/k_B$ , which is a very high temperature. Here we argue that the upper bound temperature for the power-law behavior of  $\sigma_{\perp}(V, T)$  in Eq. (14) is much lower, due to the presence of marginal and irrelevant couplings (inelastic scattering with phonons, etc.). Note that  $\sigma_{\perp}(V,T)$  in Eq. (13) considers only the relevant bare coupling  $\widetilde{t}_{\perp}$ , which has the unit of energy. In general, irrelevant couplings of dimension  $-\Delta < 0$  would induce effective couplings scaling as  $(k_B T)^{\Delta}$ , which grow as T increases. Without a detailed knowledge of the irrelevant couplings, we expect their corrections to be no longer negligible when  $k_BT > \tilde{t}_{\perp}$ . This sets an upper bound crossover temperature for the SLL behavior as

$$T_0 \sim k_B^{-1} \widetilde{t}_\perp, \tag{15}$$

which we adopt here. The SLL regime is thus within the temperature range  $T_* < T < T_0$ .

Figure 3(c) shows the lower bound temperature  $T_*$  as a function of twist angle  $\theta$  for  $E_F=30$  meV and interaction strength U ranging from 0 to 4eV, for which the Luttinger liquid parameter  $g_{\rm eff}$  is shown in Fig. 2(b). Generically, we find that  $T_*$  decreases as  $\theta$  decreases, because of the decrease of  $\widetilde{t}_{\perp}$ , although  $g_{\rm eff}$  increases. As an example, Fig. 3(d) shows the phase diagram plotted for  $E_F=30$  meV, U=3 eV with respect to  $\theta$ , where the lower and upper curves are the crossover temperatures  $T_*$  in Eq. (12) and  $T_0$  and Eq. (15),

respectively, between which is the SLL regime. We note that  $T_*$  and  $T_0$  are both order estimations. At temperatures  $T>T_0$ , one expects the anisotropy of the system to be suppressed by strong thermal fluctuations and irrelevant couplings, which we call the isotropic regime. For temperatures  $T< T_*$  which we denote as the 2D regime, the perpendicular hopping  $\widetilde{t}_\perp$  becomes important, and the system will behave intrinsically as a low temperature 2D system. As the temperature T decreases, depending on interactions, the system may remain a 2D Fermi liquid till T=0, or undergo a symmetry breaking phase transition into charge density wave, etc., as studied in the literature [8–11].

Discussion. We have seen that, for the effective coupled moiré wires, the Luttinger parameter  $g_{\rm eff}$  (e.g.,  $\sim$ 0.3 for U=3 eV) is much lower than the Luttinger parameter g ( $\sim$ 0.6 for U=3 eV, see SM [49] Sec. III) of the monolayer microscopic coupled wires. Generically, this is because of the lowering of Fermi velocity  $v_F$  and effectively longer range of interaction broadened by the widths of moiré wires. The lower bound temperature  $T_*$  of the SLL regime can be rather sensitive to U. For our parameters, at  $\theta=5^\circ$ ,  $T_*$  drops from 50 K to about

- 4 K as U increases from 2 to 4 eV. If U further increases,  $T_*$  would drop down to zero, leading to a zero-temperature SLL quantum phase. In the WTe<sub>2</sub> experiments [28,29],  $T_* \sim 2$  K at  $\theta = 5^{\circ}$ , and  $T_* < 50$  mK at  $\theta = 3^{\circ}$ , which are similar to our results for  $U \gtrsim 3$  eV. This suggests that a strong microscopic interaction is needed to explain the experiments. Future studies with more accurate moiré models are needed for quantitative understandings. More generally, we expect our twisted coupled wire modeling to be applicable to twisted bilayers of 2D anisotropic systems, such as arrays of nanowires [5,6], black phosphorus [66], etc., with different energy scales.
- Acknowledgments. We are thankful for the helpful discussions with Tiancheng Song, Guo Yu, Pengjie Wang, Sanfeng Wu, and Jing Wang. This work is supported by the Alfred P. Sloan Foundation, by the National Science Foundation under award (DMR-2141966) and (DMR-2011750) through the Princeton University's Materials Research Science and Engineering Center. Additional support was provided by the Gordon and Betty Moore Foundation through Grant No. GBMF8685 towards the Princeton theory program.
- S.-I. Tomonaga, Remarks on Bloch's method of sound waves applied to many-fermion problems, Prog. Theor. Phys. 5, 544 (1950).
- [2] F. D. M. Haldane, 'Luttinger liquid theory' of one-dimensional quantum fluids. I. Properties of the Luttinger model and their extension to the general 1D interacting spinless Fermi gas, J. Phys. C 14, 2585 (1981).
- [3] J. M. Luttinger, An exactly soluble model of a many-fermion system, J. Math. Phys. 4, 1154 (1963).
- [4] T. Giamarchi, Quantum Physics in One Dimension (Oxford University Press, Oxford, 2003).
- [5] S. Wang, S. Zhao, Z. Shi, F. Wu, Z. Zhao, L. Jiang, K. Watanabe, T. Taniguchi, A. Zettl, C. Zhou, and F. Wang, Nonlinear Luttinger liquid plasmons in semiconducting single-walled carbon nanotubes, Nat. Mater. 19, 986 (2020).
- [6] Y. Jompol, C. J. B. Ford, J. P. Griffiths, I. Farrer, G. A. C. Jones, D. Anderson, D. A. Ritchie, T. W. Silk, and A. J. Schofield, Probing spin-charge separation in a Tomonaga-Luttinger liquid, Science 325, 597 (2009).
- [7] X. G. Wen, Metallic non-Fermi-liquid fixed point in two and higher dimensions, Phys. Rev. B 42, 6623 (1990).
- [8] V. J. Emery, E. Fradkin, S. A. Kivelson, and T. C. Lubensky, Quantum theory of the smectic metal state in stripe phases, Phys. Rev. Lett. 85, 2160 (2000).
- [9] S. L. Sondhi and K. Yang, Sliding phases via magnetic fields, Phys. Rev. B 63, 054430 (2001).
- [10] A. Vishwanath and D. Carpentier, Two-dimensional anisotropic non-Fermi-liquid phase of coupled luttinger liquids, Phys. Rev. Lett. 86, 676 (2001).
- [11] R. Mukhopadhyay, C. L. Kane, and T. C. Lubensky, Sliding Luttinger liquid phases, Phys. Rev. B 64, 045120 (2001).
- [12] J. C. Y. Teo and C. L. Kane, From Luttinger liquid to non-Abelian quantum Hall states, Phys. Rev. B **89**, 085101 (2014).
- [13] C. L. Kane, A. Stern, and B. I. Halperin, Pairing in Luttinger liquids and quantum Hall states, Phys. Rev. X 7, 031009 (2017).

- [14] Y. Fuji and P. Lecheminant, Non-Abelian SU(N-1)-singlet fractional quantum Hall states from coupled wires, Phys. Rev. B **95**, 125130 (2017).
- [15] C. L. Kane and A. Stern, Coupled wire model of Z<sub>4</sub> orbifold quantum Hall states, Phys. Rev. B 98, 085302 (2018).
- [16] Y. Imamura, K. Totsuka, and T. H. Hansson, From coupled-wire construction of quantum Hall states to wave functions and hydrodynamics, Phys. Rev. B 100, 125148 (2019).
- [17] P. M. Tam, Y. Hu, and C. L. Kane, Coupled wire model of  $Z_2 \times Z_2$  orbifold quantum Hall states, Phys. Rev. B **101**, 125104 (2020).
- [18] P. M. Tam and C. L. Kane, Nondiagonal anisotropic quantum Hall states, Phys. Rev. B 103, 035142 (2021).
- [19] T. Neupert, C. Chamon, C. Mudry, and R. Thomale, Wire deconstructionism of two-dimensional topological phases, Phys. Rev. B 90, 205101 (2014).
- [20] T. Iadecola, T. Neupert, C. Chamon, and C. Mudry, Wire constructions of Abelian topological phases in three or more dimensions, Phys. Rev. B 93, 195136 (2016).
- [21] Y. Fuji and A. Furusaki, From coupled wires to coupled layers: Model with three-dimensional fractional excitations, Phys. Rev. B 99, 241107(R) (2019).
- [22] T. Meng, T. Neupert, M. Greiter, and R. Thomale, Coupled-wire construction of chiral spin liquids, Phys. Rev. B 91, 241106(R) (2015).
- [23] A. A. Patel and D. Chowdhury, Two-dimensional spin liquids with z<sub>2</sub> topological order in an array of quantum wires, Phys. Rev. B 94, 195130 (2016).
- [24] J. C. Y. Teo and Y. Hu, Dihedral twist liquid models from emergent Majorana fermions, Quantum 7, 967 (2023).
- [25] A. Georges, T. Giamarchi, and N. Sandler, Interchain conductivity of coupled Luttinger liquids and organic conductors, Phys. Rev. B 61, 16393 (2000).
- [26] X. Du, L. Kang, Y. Y. Lv, J. S. Zhou, X. Gu, R. Z. Xu, Q. Q. Zhang, Z. X. Yin, W. X. Zhao, Y. D. Li, S. M. He, D. Pei, Y. B. Chen, M. X. Wang, Z. K. Liu, Y. L. Chen, and L. X. Yang,

- Crossed Luttinger liquid hidden in a quasi-two-dimensional material, Nat. Phys. 19, 40 (2023).
- [27] L. Niu, S. Jin, X. Chen, X. Li, and X. Zhou, Observation of a dynamical sliding phase superfluid with *p*-band bosons, Phys. Rev. Lett. **121**, 265301 (2018).
- [28] P. Wang, G. Yu, Y. H. Kwan, Y. Jia, S. Lei, S. Klemenz, F. A. Cevallos, R. Singha, T. Devakul, K. Watanabe, T. Taniguchi, S. L. Sondhi, R. J. Cava, L. M. Schoop, S. A. Parameswaran, and S. Wu, One-dimensional Luttinger liquids in a two-dimensional moiré lattice, Nature (London) 605, 57 (2022).
- [29] G. Yu, P. Wang, A. J. Uzan-Narovlansky, Y. Jia, M. Onyszczak, R. Singha, X. Gui, T. Song, Y. Tang, K. Watanabe, T. Taniguchi, R. J. Cava, L. M. Schoop, and S. Wu, Evidence for two dimensional anisotropic Luttinger liquids at millikelvin temperatures, Nat. Commun. 14, 7025 (2023).
- [30] L. Balents, C. R. Dean, D. K. Efetov, and A. F. Young, Superconductivity and strong correlations in moiré flat bands, Nat. Phys. 16, 725 (2020).
- [31] F. Haddadi, Q. Wu, A. J. Kruchkov, and O. V. Yazyev, Moiré flat bands in twisted double bilayer graphene, Nano Lett. **20**, 2410 (2020).
- [32] H. Li, S. Li, M. H. Naik, J. Xie, X. Li, J. Wang, E. Regan, D. Wang, W. Zhao, S. Zhao, S. Kahn, K. Yumigeta, M. Blei, T. Taniguchi, K. Watanabe, S. Tongay, A. Zettl, S. G. Louie, F. Wang, and M. F. Crommie, Imaging moiré flat bands in three-dimensional reconstructed WSe<sub>2</sub>/WS<sub>2</sub> superlattices, Nat. Mater. 20, 945 (2021).
- [33] Y. Tang, L. Li, T. Li, Y. Xu, S. Liu, K. Barmak, K. Watanabe, T. Taniguchi, A. H. MacDonald, J. Shan, and K. F. Mak, Simulation of Hubbard model physics in WSe<sub>2</sub>/WS<sub>2</sub> moiré superlattices, Nature (London) 579, 353 (2020).
- [34] F. Wu, T. Lovorn, E. Tutuc, and A. H. MacDonald, Hubbard model physics in transition metal dichalcogenide moiré bands, Phys. Rev. Lett. **121**, 026402 (2018).
- [35] Y. Shimazaki, I. Schwartz, K. Watanabe, T. Taniguchi, M. Kroner, and A. Imamoğlu, Strongly correlated electrons and hybrid excitons in a moiré heterostructure, Nature (London) 580, 472 (2020).
- [36] E. C. Regan, D. Wang, C. Jin, M. I. B. Utama, B. Gao, X. Wei, S. Zhao, W. Zhao, Z. Zhang, K. Yumigeta, M. Blei, J. D. Carlström, K. Watanabe, T. Taniguchi, S. Tongay, M. Crommie, A. Zettl, and F. Wang, Mott and generalized Wigner crystal states in WSe<sub>2</sub>/WS<sub>2</sub> moiré superlattices, Nature (London) 579, 359 (2020).
- [37] M. Yankowitz, S. Chen, H. Polshyn, Y. Zhang, K. Watanabe, T. Taniguchi, D. Graf, A. F. Young, and C. R. Dean, Tuning superconductivity in twisted bilayer graphene, Science 363, 1059 (2019).
- [38] X. Liu, Z. Hao, E. Khalaf, J. Y. Lee, Y. Ronen, H. Yoo, D. H. Najafabadi, K. Watanabe, T. Taniguchi, A. Vishwanath, and P. Kim, Tunable spin-polarized correlated states in twisted double bilayer graphene, Nature (London) 583, 221 (2020).
- [39] K. Kim, A. DaSilva, S. Huang, B. Fallahazad, S. Larentis, T. Taniguchi, K. Watanabe, B. J. LeRoy, A. H. MacDonald, and E. Tutuc, Tunable moiré bands and strong correlations in small-twist-angle bilayer graphene, Proc. Natl. Acad. Sci. 114, 3364 (2017).
- [40] X. Lu, P. Stepanov, W. Yang, M. Xie, M. A. Aamir, I. Das, C. Urgell, K. Watanabe, T. Taniguchi, G. Zhang, A. Bachtold,

- A. H. MacDonald, and D. K. Efetov, Superconductors, orbital magnets and correlated states in magic-angle bilayer graphene, Nature (London) **574**, 653 (2019).
- [41] Y. Cao, V. Fatemi, A. Demir, S. Fang, S. L. Tomarken, J. Y. Luo, J. D. Sanchez-Yamagishi, K. Watanabe, T. Taniguchi, E. Kaxiras, R. C. Ashoori, and P. Jarillo-Herrero, Correlated insulator behaviour at half-filling in magic-angle graphene superlattices, Nature (London) 556, 80 (2018).
- [42] Y. Cao, V. Fatemi, S. Fang, K. Watanabe, T. Taniguchi, E. Kaxiras, and P. Jarillo-Herrero, Unconventional superconductivity in magic-angle graphene superlattices, Nature (London) 556, 43 (2018).
- [43] G. W. Burg, J. Zhu, T. Taniguchi, K. Watanabe, A. H. MacDonald, and E. Tutuc, Correlated insulating states in twisted double bilayer graphene, Phys. Rev. Lett. 123, 197702 (2019).
- [44] Y. Cao, D. Rodan-Legrain, O. Rubies-Bigorda, J. M. Park, K. Watanabe, T. Taniguchi, and P. Jarillo-Herrero, Tunable correlated states and spin-polarized phases in twisted Bilayer— Bilayer graphene, Nature (London) 583, 215 (2020).
- [45] G. Chen, L. Jiang, S. Wu, B. Lyu, H. Li, B. L. Chittari, K. Watanabe, T. Taniguchi, Z. Shi, J. Jung, Y. Zhang, and F. Wang, Evidence of a gate-tunable Mott insulator in a trilayer graphene moiré superlattice, Nat. Phys. 15, 237 (2019).
- [46] C.-H. Hsu, D. Loss, and J. Klinovaja, General scattering and electronic states in a quantum-wire network of moiré systems, Phys. Rev. B **108**, L121409 (2023).
- [47] M. Angeli and A. H. MacDonald, Γ valley transition metal dichalcogenide moiré bands, Proc. Natl. Acad. Sci. USA 118, e2021826118 (2021).
- [48] S. Fang, R. Kuate Defo, S. N. Shirodkar, S. Lieu, G. A. Tritsaris, and E. Kaxiras, *Ab initio* tight-binding Hamiltonian for transition metal dichalcogenides, Phys. Rev. B **92**, 205108 (2015).
- [49] See Supplemental Material at http://link.aps.org/supplemental/ 10.1103/PhysRevB.110.L201106 for details regarding calculations of transfer matrix, Fourier components of interaction potential, monolayer Luttinger liquid parameter estimations and interlayer hopping parameter and strength estimations.
- [50] G. Kresse and J. Furthmüller, Efficiency of *ab-initio* total energy calculations for metals and semiconductors using a plane-wave basis set, Comput. Mater. Sci. 6, 15 (1996).
- [51] G. Kresse and J. Hafner, Ab initio molecular dynamics for openshell transition metals, Phys. Rev. B 48, 13115 (1993).
- [52] J. P. Perdew, K. Burke, and M. Ernzerhof, Generalized gradient approximation made simple, Phys. Rev. Lett. 77, 3865 (1996).
- [53] B. Sun, W. Zhao, T. Palomaki, Z. Fei, E. Runburg, P. Malinowski, X. Huang, J. Cenker, Y.-T. Cui, J.-H. Chu, X. Xu, S. S. Ataei, D. Varsano, M. Palummo, E. Molinari, M. Rontani, and D. H. Cobden, Evidence for equilibrium exciton condensation in monolayer WTe<sub>2</sub>, Nat. Phys. 18, 94 (2022).
- [54] Y. Jia, P. Wang, C.-L. Chiu, Z. Song, G. Yu, B. Jäck, S. Lei, S. Klemenz, F. A. Cevallos, M. Onyszczak, N. Fishchenko, X. Liu, G. Farahi, F. Xie, Y. Xu, K. Watanabe, T. Taniguchi, B. A. Bernevig, R. J. Cava, L. M. Schoop *et al.*, Evidence for a monolayer excitonic insulator, Nat. Phys. 18, 87 (2022).
- [55] R. Jing, Y. Shao, Z. Fei, C. F. B. Lo, R. A. Vitalone, F. L. Ruta, J. Staunton, W. J.-C. Zheng, A. S. Mcleod, Z. Sun, B. yuan Jiang, X. Chen, M. M. Fogler, A. J. Millis, M. Liu, D. H. Cobden, X. Xu, and D. N. Basov, Terahertz response of monolayer

- and few-layer WTe<sub>2</sub> at the nanoscale, Nat. Commun. **12**, 5594 (2021).
- [56] J. Kwak, Y. Jo, S. Song, J. H. Kim, S.-Y. Kim, J.-U. Lee, S. Lee, J. Park, K. Kim, G.-D. Lee, J.-W. Yoo, S. Y. Kim, Y.-M. Kong, G.-H. Lee, W.-G. Lee, J. Park, X. Xu, H. Cheong, E. Yoon, Z. Lee *et al.*, Single-crystalline nanobelts composed of transition metal ditellurides, Adv. Mater. 30, 1707260 (2018).
- [57] G.-B. Liu, D. Xiao, Y. Yao, X. Xu, and W. Yao, Electronic structures and theoretical modelling of two-dimensional group-VIB transition metal dichalcogenides, Chem. Soc. Rev. 44, 2643 (2015).
- [58] V. Crépel and L. Fu, Spin-triplet superconductivity from excitonic effect in doped insulators, Proc. Natl. Acad. Sci. USA 119, 117735119 (2022).
- [59] S. Tang, C. Zhang, D. Wong, Z. Pedramrazi, H.-Z. Tsai, C. Jia, B. Moritz, M. Claassen, H. Ryu, S. Kahn, J. Jiang, H. Yan, M. Hashimoto, D. Lu, R. G. Moore, C.-C. Hwang, C. Hwang, Z. Hussain, Y. Chen, M. M. Ugeda *et al.*, Quantum spin Hall state in monolayer 1T'-WTe<sub>2</sub>, Nat. Phys. 13, 683 (2017).
- [60] Y. H. Kwan, T. Devakul, S. L. Sondhi, and S. A. Parameswaran, Theory of competing excitonic orders in insulating WTe<sub>2</sub> monolayers, Phys. Rev. B 104, 125133 (2021).

- [61] A. N. Domozhirova, A. A. Makhnev, E. I. Shreder, S. V. Naumov, A. V. Lukoyanov, V. V. Chistyakov, J. C. A. Huang, A. A. Semiannikova, P. S. Korenistov, and V. V. Marchenkov, Electronic properties of WTe<sub>2</sub> and MoTe<sub>2</sub> single crystals, J. Phys.: Conf. Ser. 1389, 012149 (2019).
- [62] M. P. A. Fisher and L. I. Glazman, Transport in a onedimensional Luttinger liquid, in *Mesoscopic Electron Transport* (Springer Netherlands, Amsterdam, 1997), pp. 331–373.
- [63] C. Bourbonnais, F. Creuzet, D. Jérome, K. Bechgaard, and A. Moradpour, Cooperative phenomena in (TMTSF)2ClO4: an NMR evidence, J. Phys. Lett. 45, 755 (1984).
- [64] E. Fradkin, Field Theories of Condensed Matter Physics (Cambridge University Press, Cambridge, 2013).
- [65] S. Biermann, A. Georges, T. Giamarchi, and A. Lichtenstein, Quasi one-dimensional organic conductors: Dimensional crossover and some puzzles, in *Strongly Correlated Fermions* and Bosons in Low-Dimensional Disordered Systems (Springer Netherlands, Amsterdam, 2002), pp. 81–102.
- [66] H. Wang, Z. Liu, Y. Jiang, and J. Wang, Giant anisotropic band flattening in twisted Γ-valley semiconductor bilayers, Phys. Rev. B 108, L201120 (2023).